ADVANCED ENERGY MATERIALS
www.advenergymat.de

Device Characteristics of CZTSSe Thin-Film Solar Cells with 12.6% Efficiency

*Wei Wang, Mark T. Winkler, Oki Gunawan, Tayfun Gokmen, Teodor K. Todorov, Yu Zhu, and David B. Mitzi**

The thin-film photovoltaic material $Cu_2ZnSnS_xSe_{4-x}$ (CZTSSe) has drawn world-wide attention due to its outstanding performance and earth-abundant composition. Until recently,[1] state-of-the-art CZTSSe thin-film solar cells were limited to 11.1% power conversion efficiency (PCE), with these performance levels being achieved via a hydrazine slurry approach.[2] Other vacuum- and non-vacuum-based deposition techniques have also been successful in fabricating CZTSSe solar cells with PCE above 8%.[3,4] However, even record devices with PCE of 11% are still far below the physical limit, known as the Shockley-Queisser (SQ) limit, of about 31% efficiency under terrestrial conditions.[5]

For a solar cell with 1.13 eV bandgap such as the previous 11.1% champion,[2] the SQ limits for open circuit voltage (V_{oc}) and short-circuit current density (J_{sc}) are 820 mV and 43.4 mA cm^{-2}, respectively. The previous 11.1% champion only achieved a V_{oc} of 460 mV and a J_{sc} of 34.5 mA cm^{-2}, corresponding to about 56% and 79% of the SQ limit values. In order to boost J_{sc}, an optical architecture with optimized transparent conductive oxide (TCO) and CdS thicknesses has recently been reported, leading to a new CZTSSe record PCE of 12.0% and a J_{sc} that reaches 83% of the SQ limit.[1] Despite improvements in short-circuit current, the V_{oc} deficit, equal to the difference between the bandgap and V_{oc}, is currently the biggest hurdle preventing CZTSSe devices from achieving higher efficiency.[6] Enhancement of V_{oc} also directly improves device fill factor.[7] Although many factors can influence V_{oc} in a solar cell, carrier generation and recombination near the charge-separating junction play a dominant role. Thus, in order to decrease the V_{oc} deficit and increase efficiency beyond 12%, it is critical to understand junction characteristics, current collection, and recombination mechanisms in the current generation of devices.

Here, an independently certified world-record 12.6% PCE CZTSSe thin-film solar cell is presented. The new champion device was fabricated using a recently described hydrazine pure-solution approach, targeting a Cu-poor and Zn-rich condition.[8] Secondary ion mass spectrometry (SIMS) shows that the obtained CZTSSe films exhibit very low carbon and oxygen concentrations, comparable to films fabricated by the more traditional hydrazine-slurry method.[9] The rheological properties of the particle-free solution, relative to the slurry process, significantly improves the coating uniformity and film structure and, consequently, the performance of the solar cells.[4,8] By simultaneously optimizing the TCO and CdS thicknesses to maximize photon transmission to the absorber and improving the bulk qualities of CZTSSe with the hydrazine pure-solution approach, both J_{sc} and V_{oc} are boosted in the 12.6% champion device. Device characteristics of the new champion cell, as deduced from current–voltage, quantum efficiency, capacitance, and electron-beam-induced current (EBIC) measurements, are discussed in detail, thereby providing fundamental information regarding the photovoltaic characteristics of CZTS/CdS heterojunctions in devices with efficiency of over 12%.

The CZTSSe absorber layers were characterized by electron microscopy and energy-dispersive X-ray spectroscopy (EDX) to investigate CZTSSe-morphologic and compositional properties. Top-view and cross-sectional scanning electron microscopy (SEM) images of CZTSSe films fabricated from the hydrazine pure-solution approach are shown in **Figure 1**. The CZTSSe film thickness is estimated to be 2 μm with micrometer-sized grains. Overall, the film is dense and pinhole-free, with a few voids visible at the CZTSSe-Mo interface. The molybdenum back contact is about 500-nm thick with 185 nm ± 30 nm of $Mo(S,Se)_2$ forming at the interface with the CZTSSe during thermal annealing. The $Mo(S,Se)_2$ layer thickness is substantially thinner than earlier generation devices with efficiency under 10% (≈300 nm thickness for these devices).[9] In **Figure 2**a, EDX compositional profiling across the CZTSSe film thickness shows uniform elemental distribution in the bulk, with slight compositional drift near the Mo back contact and a detectable amount of copper in the $Mo(S,Se)_2$ layer. The presence of copper in $Mo(S,Se)_2$ was confirmed by SIMS of the same sample (Supporting Information Figure S1), where copper signals plateau in $Mo(S,Se)_2$ as well as exhibiting a much longer decay than zinc and tin signals. In Figure 2b, EDX compositional scanning shows uniform elemental profiles of Cu, Zn, and Sn in the region of the CdS/CZTSSe junction. Other EDX images (shown in Supporting Information Figure S2) show that small Zn(S,Se) grains co-exist at the top surface of the CZTSSe films. For future work, the compositional homogeneity and phase purity in the absorber may need to be more finely controlled in order to further increase power conversion efficiency.

To assess progress in CZTSSe solar cells, it is illuminating to compare the state-of-the-art devices with comparable CIGS devices. **Table 1** presents a summary of the device characteristics of the current CZTSSe champion cell labeled "D1". For

Dr. W. Wang, Dr. M. T. Winkler, Dr. O. Gunawan, Dr. T. Gokmen, Dr. T. K. Todorov, Dr. Y. Zhu, Dr. D. B. Mitzi
IBM T. J. Watson Research Center
P. O. Box 218, Yorktown Heights, NY, 10598, USA
E-mail: dmitzi@us.ibm.com

DOI: 10.1002/aenm.201301465

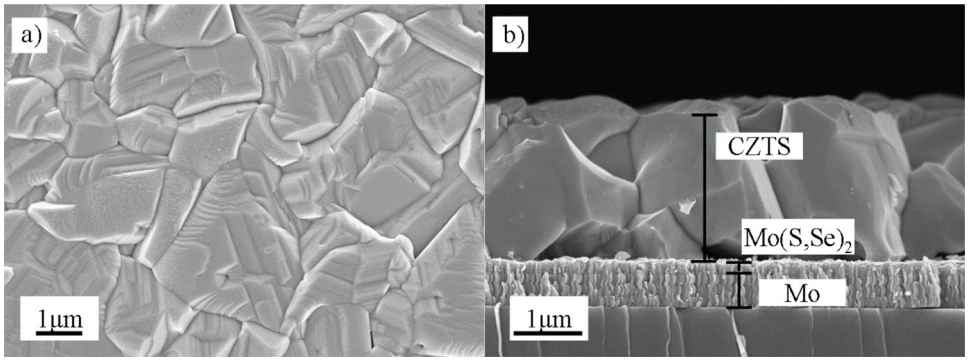

Figure 1. a) Top-view and b) cross-sectional view SEM images of a sister CZTSSe film to the 12.6% record device.

reference and comparison we also include the previous 11.1% champion device labeled "C1",[2] and two champion CIGSSe devices: an IBM CIGSSe device processed with similar hydrazine-based processing yielding 15.2% efficiency and a record ZSW (Zentrum für Sonnenenergie- und Wasserstoff) CIGSSe device with 20.3% efficiency.[11,12] **Figure 3** shows the current–voltage (*J*–*V*) characteristics of the current champion cell D1 along with the quantum efficiency (QE) and the reflectivity spectra. The QE data allow us to estimate the band gap (E_g) of the absorber layer using the inflection point of the QE curves near the absorption edge as indicated by the dashed line. Both champion CZTSSe cells D1 and C1 have the same band gap of 1.13 eV, thus facilitating straightforward comparison between their device characteristics. As seen in Table 1, the current champion cell improves in J_{sc} by 0.7 mA cm^{-2} (or 2%) and more significantly in V_{oc} by 54 mV (or 11.6%) relative to the previous champion cell C1. However the *FF* remains the same, despite the V_{oc} increase, evidently due to higher series resistance in cell D1 (R_{SL} = 0.72 Ω cm^2). The diode ideality factor in the champion CZTSSe cell (A = 1.45) has also improved to a value close to that for the ZSW-CIGSSe champion device (A = 1.38), consistent with the improvement in V_{oc} that suggests less recombination in the space-charge region (either interface or bulk).

Future progress in CZTSSe solar cells will likely rely on understanding the defect or defects that lower V_{oc} relative to its ideal value;[13] capacitance profiling offers insight into the concentration and nature of defects near the CZTSSe/CdS heterojunction. **Figure 4**a shows a capacitance–voltage (*C*–*V*) sweep and drive level capacitance profiling (DLCP) study for both the record CZTSSe device D1 and the IBM-CIGSSe devices. In general, DLCP is sensitive only to the bulk defects while *C*–*V* is also sensitive to the interface traps.[14] The drive level densities (N_{DL}) are similar for both samples ($N_{DL} < 7 \times 10^{15}$ cm^{-3}), except that the depletion width (at zero bias) in the CZTSSe device D1 is shorter ($x_d \approx 0.15$ μm vs 0.27 μm for the CIGSSe device). Furthermore, in CZTSSe, the *C*–*V* curve is shifted to significantly higher values than the DLCP curve, while in the CIGSSe cell they are in closer agreement. The difference (e.g., at zero bias) for the CZTSSe device presumably arises from the presence of traps at the CZTSSe/CdS interface (N_{IT}).[14,15] According to the capacitance data, N_{IT} is larger in CZTSSe than in the CIGS device. The larger value of N_{IT} likely contributes to the suppressed 0-K intercept for the V_{oc} vs. T profile (i.e., the activation energy of the main recombination process, E_A) (Supporting Information Figure S4). In general for CZTSSe devices, the fact that $E_A < E_g$ is interpreted as evidence for a high recombination rate at the CdS/CZTSSe interface.[16,17]

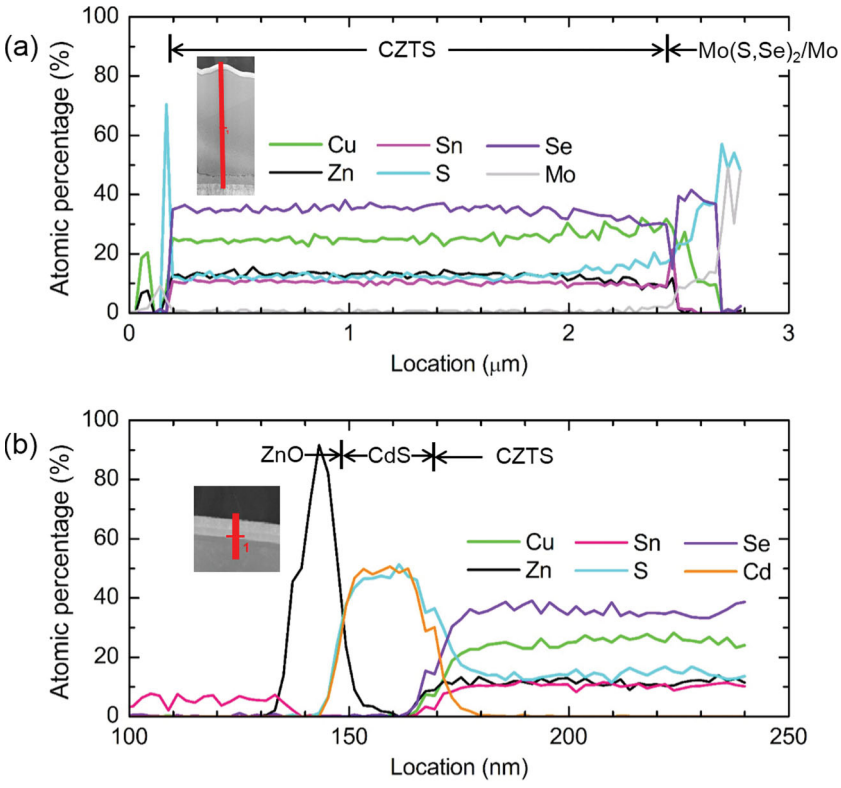

Figure 2. EDX analysis on a 12% CZTSSe device (a sister sample to the 12.6% efficiency device): a) across the thickness of CZTSSe layer and b) across the CdS/CZTSSe junction. The insets show the physical path for the EDX scanning in the STEM images.

Table 1. Device characteristics of the current champion CZTSSe cell (D1) compared to a previous record cell (C1, see ref. [2]), and two champion CIGSSe cells (IBM-CIGSSe[11] and ZSW-CIGSSe[12]). Values marked by * are measured and certified by Newport Corporation (see Supporting Information Figure S3 for the certificate of D1). The diode parameters, series resistance under light (R_{SL}), shunt conductance under light (G_{SL}), ideality factor (A), and reverse saturation current (J_0), are determined using the Sites' method.[10] The A values in parentheses are determined from J_{sc}–V_{oc} data in separate measurement after certification.

Cell	Efficiency [%]	FF [%]	V_{oc} [mV]	J_{sc} [mA cm^{-2}]	R_{SL} [Ω cm^2]	G_{SL} [mS cm^{-2}]	A	J_0 [A cm^{-2}]	E_g [eV]	E_g/q–V_{oc} [V]
D1 (CZTSSe)	12.6*	69.8*	513.4*	35.2*	0.72	1.61	1.45 (1.24)	7.0×10^{-8}	1.13	0.617
C1 (CZTSSe)	11.1*	69.8*	459.8*	34.5*	0.40	1.70	1.48 (1.28)	2.2×10^{-7}	1.13	0.670
IBM-CIGSSe	15.2*	75.1*	623.1*	32.6*	0.38	0.39	1.49(1.37)	3.7×10^{-9}	1.17	0.547
ZSW-CIGSSe	20.3	77.7	730	35.7	0.23	1.14	1.38	4.2×10^{-11}	1.14	0.410

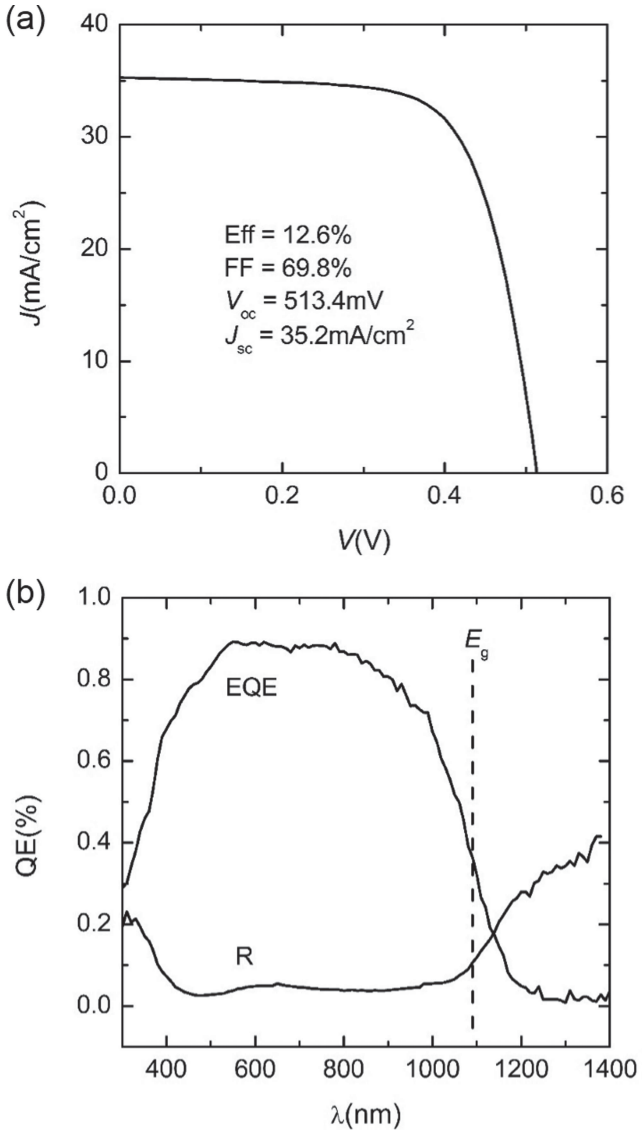

Figure 3. a) J–V characteristics of the record device (from Newport certification). b) EQE and reflectivity (R) spectra. The dashed line marks the bandgap extracted from the inflection of the EQE curve.

Although we can not rule out the influence of bulk defects in CZTSSe films, and indeed recent measurements suggest the importance of tail states in reducing V_{oc},[18] passivating interface defects may represent one additional important focal point for achieving higher performing solar cells.

Regardless of their origin (interface or bulk), defects in the vicinity of the CZTSSe/CdS heterojunction impact the carrier lifetime, and thus the diffusion length and collection efficiency of minority carriers generated in the absorber layer. Both of these latter parameters can be directly examined in Figure 4b, which presents the cross-sectional SEM and electron beam induced current (EBIC) measurement for a sister cell of the champion device (i.e., also exhibiting efficiency of >12%). Bright areas in the EBIC image indicate regions of high collection efficiency for minority carriers. The image clearly shows that collection within 1 μm of the CZTSSe/CdS junction occurs with relatively high grain-to-grain uniformity (given expected geometrical issues associated with the rough cleaved surface), which is essential for high performing devices.[19] The collection region in a p–n junction solar cell has contributions both from the depletion width (x_d) and diffusion length (L_d) and therefore the collection depth should be roughly equal to $x_d + L_d$. Although some non-uniformities exist (perhaps partially due to geometric effects in the cleaved sample and from the variation in the junction quality), the extent of the collection depth measured from the junction indicates $x_d + L_d \approx 1$ μm. Indeed, by measuring the voltage dependence of the IQE data,[20] we deduce that $L_d = 0.75$ μm ± 0.15 μm. In addition, the DLCP data of Figure 4a indicate that $x_d = 0.15$ μm ± 0.03 μm. Combining the L_d measurement from the IQE data and the x_d measurement from the capacitance data ($x_d + L_d = 0.9$), we obtain a value consistent with that derived from the EBIC measurement on cleaved samples. We also estimate the potential improvement in J_{sc} in the scenario of a CZTSSe device with a larger $L_d = 2$ μm (a value comparable to high-performance CIGS),[20] while keeping the depletion width the same. Our calculations show that the expected increase in J_{sc} would be ≈2 mA cm^{-2}, which corresponds to an absolute gain of 0.7% in efficiency (assuming constant V_{oc}). Therefore, improving the diffusion length of minority carriers (e.g., by addressing the relatively low mobility and lifetime) represents a potential pathway to increase efficiency beyond 13%.

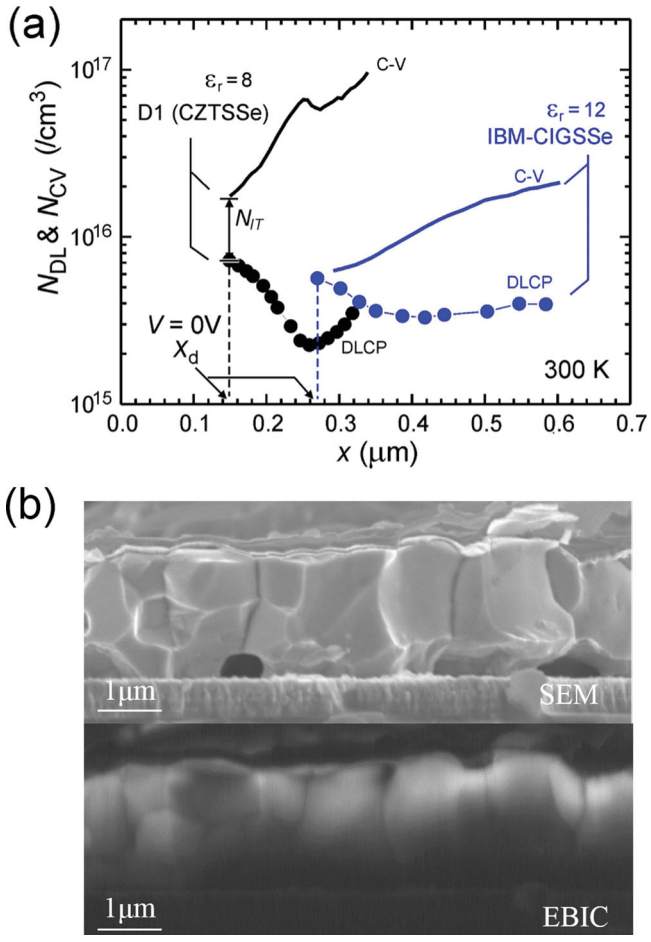

Figure 4. a) *C–V* and DLCP characteristics of cell D1 and IBM-CIGSSe at 300 K. The *C–V* is performed using 50-mV, 100-kHz ac excitation with dc bias from 0 to –5 V, and DLCP is performed using 100-kHz ac excitation with amplitude from 20 to 200 mV and with dc bias from 0 to –5 V. ε_r is the relative dielectric constant. b) Cross-sectional SEM and EBIC images for a cleaved high-performance CZTSSe device.

Although improvements in V_{oc} represent the largest potential improvement in CZTSSe efficiency, J_{sc} can also be improved significantly relative to the previous 11.1% champion with the same band gap. For example, efficiency could improve 3–5% (absolute) through superior photon management.[1] As discussed in reference[1], the optical architecture of previous champion CZTSSe devices was sub-optimal; moreover, the typical approach to solar cell photon management, minimizing reflectivity, does not yield optimal results in CZTSSe. Rather, due to the absorbing nature of the top layers of the device (CdS and TCO), a tradeoff exists between minimizing reflectivity from the active surface of the device (which favors thicker CdS) and minimizing absorption in the top-layers of the device (which favors thinner CdS). In pratice, the CdS layer should be as thin as possible, provided it still creates a satisfactory rectifying junction with the CZTSSe-absorber layer. We have recently shown via both optical modeling of idealized, planar device models as well as empirical studies that J_{sc} can be improved relative to the 11.1% champion by utilizing thinner CdS and TCO layers. For example, a device architecture that utilizes a CdS thickneses of about 25 nm and a TCO thickness of about 50 nm yields a 10% improvement in J_{sc} relative to the 11.1% (60 nm CdS and 240 nm) device. However, the current champion device only exhibited a 2% enhancement over the previous champion with the same band gap, most likely at least in part as a result of a deviation of CdS and TCO thicknesses from targeted values.

In summary, a 12.6%-efficiency CZTSSe solar cell fabricated by a hydrazine pure-solution process has been presented, with improvements in both V_{oc} (11.6%) and J_{sc} (2%) relative to an analogous 11.1% device with the same band gap. The resulting reduction in V_{oc} deficit by ≈50 mV leads to the smallest V_{oc}-deficit value yet achieved for this range of CZTSSe band gaps. The discrepancy between *C-V* and DLCP curves at zero bias, as well as suppression of the 0-K intercept for the V_{oc} vs. *T* profile (i.e., the activation energy of the main recombination process, E_A) below the CZTSSe band gap value, suggest that there may still be a substantial component of interfacial recombination within the record device, representing at least one route through which V_{oc} deficit might be further improved. Key device parameters have been reported for devices with efficiency >12%, including the depletion width x_d (0.15 μm ± 0.03 μm), the diffusion length L_d (0.75 μm ± 0.15 μm) and the drive-level density N_{DL} (<7×10^{15} cm^{-3}). The 1-μm current-collection depth deduced from EBIC is in good agreement with the value calculated using the capacitance (depletion width) and voltage dependence of the IQE (diffusion length) data and is sufficient to collect 95% of the photogenerated carriers. We note that although optimized optical architecture for CZTSSe solar cells increases J_{sc} by approximately 10% on average,[1] the current champion device only exhibited a 2% enhancement over the previous champion with the same band gap. Further addressing this point, as well as reducing the series resistance of the device, provides a clear pathway to reaching efficiencies >13%. However, the key to more significant improvements in device performance remains further reduction of the V_{oc} deficit. Finally, the present results continue the recent trend of substantial increases in CZTSSe device performance improvements from 6.7% (2008) to 9.7% (2010) and 11.1% (2012),[2,9,21] indicating the substantial promise of this new thin-film PV materials system.

Experimental Section

Film Preparation: Caution: hydrazine is highly toxic and reactive and must be handled using appropriate protective equipment to prevent physical contact with either vapor or liquid.

The preparation of the CZTSSe films was performed using a hydrazine-based pure solution approach, following the procedures described in ref. [8] and targeting a Cu-poor and Zn-rich stoichiometry (Cu/(Zn+Sn) = 0.8 and Zn/Sn = 1.1) in the starting solution. Multiple layers of the constituent elements were spin-coated onto Mo-coated soda lime glass and annealed at a temperature in excess of 500 °C.[2,8]

Device Fabrication: CZTSSe films were deposited onto Mo-coated glass substrates, followed by standard chemical-bath deposition of 25-nm CdS and sputtering of 10-nm ZnO/50-nm ITO.[1,2,9] A 2-μm-thick Ni/Al top metal contact and 110-nm MgF_2 were deposited on top of the devices by electron-beam evaporation. The champion-cell device area (0.42 cm^2) was defined by mechanical scribing.

Characterization: Samples for SEM were coated with a Pd-Au film to prevent surface charging. Scanning transmission electron microscopy

(STEM) and EDX were conducted using an FEI Osiris with samples prepared by cryo-focused ion beam (cryoFIB) on a FEI Helios with Gatan cold stage. In-house *J–V* characterization was performed using a 6" × 6" beam Solar Simulator from Newport (with simulated AM1.5G illumination) and a Keithley 2400 sourcemeter. The system is equipped with custom-designed software that controls light stabilization and automates data acquisition using the Keithley 2400 sourcemeter. The 12.6%-efficiency device was independently certified by Newport Corporation (Calibration certificate #0857), and the performance metrics agreed with internal measurements. The *C–V* and DLCP characterizations were performed using an HP 4192 impedance analyzer (further details given in the caption of Figure 4). The quantum efficiency and reflectivity measurements were performed using a modified Protoflex system with two lock-in amplifiers for lock-in photocurrent detection from the cell under test and the light monitor. The EBIC measurement was performed on a cleaved CZTS device by MST (Foundation for Promotion of Material Science and Technology of Japan).

Supporting Information

Supporting Information is available from the Wiley Online Library or from the author.

Acknowledgements

W.W. and M.T.W. contributed equally to this work. The authors thank J. Kim for his useful discussion, S. J. Chey and R. Ferlita for their help in device fabrication, H. Hiroi and H. Sugimoto for providing substrates for this work, and M. O'Donnell from the Newport Technology and Application Center, PV Lab for PV device certification. This work was conducted as part of a joint development project between Tokyo Ohka Kogyo Co., Ltd., Solar Frontier K. K. and IBM Corporation.

Received: September 26, 2013
Revised: November 4, 2013
Published online: November 27, 2013

[1] M. T. Winkler, W. Wang, H. J. Hovel, O. Gunawan, T. K. Todorov, D. B. Mitzi, *Energy Environ. Sci.* **2013**, DOI: 10.1039/C3EE42541J.
[2] T. K. Todorov, J. Tang, S. Bag, O. Gunawan, T. Gokmen, Y. Zhu, D. B. Mitzi, *Adv. Energy Mater.* **2013**, *3*, 34.
[3] I. Repins, C. Beall, N. Vora, C. DeHart, D. Kuciauskas, P. Dippo, B. To, J. Mann, W.-C. Hsu, A. Goodrich, R. Noufi, *Sol. Energy Mater. Sol. Cells* **2012**, *101*, 154.
[4] W. Yang, H.-S. Duan, B. Bob, H. Zhou, B. Lei, C.-H. Chung, S.-H. Li, W. W. Hou, Y. Yang, *Adv. Mater.* **2012**, *24*, 6323.
[5] W. Shockley, H. J. Queisser, *J. Appl. Phys.* **1961**, *32*, 510.
[6] D. B. Mitzi, O. Gunawan, T. K. Todorov, D. A. R. Barkhouse, *Philos. Trans. R. Soc. A* **2013**, *371*, 20110432.
[7] M. Green, *Solid-State Electron.* **1981**, *24*, 788.
[8] T. K. Todorov, H. Sugimoto, O. Gunawan, T. Gokmen, D. B. Mitzi, Proc. of the 39th IEEE Photovoltaic Specialists Conference, Tampa, FL, USA, June, **2013**.
[9] T. K. Todorov, K. B. Reuter, D. B. Mitzi, *Adv. Mater.* **2010**, *22*, E156.
[10] J. R. Sites, P. H. Mauk, *Sol. Cells* **1989**, *27*, 411.
[11] T. K. Todorov, O. Gunawan, T. Gokmen, D. B. Mitzi, *Prog. Photovolt. Res. Appl.* **2013**, *21*, 82.
[12] P. Jackson, D. Hariskos, E. Lotter, S. Paetel, R. Wuerz, R. Menner, W. Wischmann, M. Powalla, *Prog. Photovolt. Res. Appl.* **2011**, *19*, 894.
[13] S. Chen, A. Walsh, X.-G. Gong, S.-H. Wei, *Adv. Mater.* **2013**, *25*, 1522.
[14] J. T. Heath, J. D. Cohen, W. N. Shafarman, *J. Appl. Phys.* **2004**, *95*, 1000.
[15] H. S. Duan, W. Yang, B. Bob, C. J. Hsu, B. Lei, Y. Yang, *Adv. Funct. Mater.* **2013**, *23*, 1466.
[16] O. Gunawan, T. K. Todorov, D. B. Mitzi, *Appl. Phys. Lett.* **2010**, *97*, 233506.
[17] V. Nadenau, U. Rau, A. Jasenek, H. W. Schock, *J. Appl. Phys.* **2000**, *87*, 584.
[18] T. Gokmen, O. Gunawan, T. K. Todorov, D. B. Mitzi, *Appl. Phys. Lett.* **2013**, *103*, 103506.
[19] I. L. Repins, H. Moutinho, S. G. Choi, A. Kanevce, D. Kuciauskas, P. Dippo, C. L. Beall, J. Carapella, C. DeHart, B. Huang, S. H. Wei, *J. Appl. Phys.* **2013**, *114*, 084507.
[20] T. Gokmen, O. Gunawan, D. B. Mitzi, *J. Appl. Phys.* **2013**, *114*, 114511.
[21] H. Katagiri, K. Jimbo, S. Yamada, T. Kamimura, W. S. Maw, T. Fukano, T. Ito, T. Motohiro, *Appl. Phys. Express* **2008**, *1*, 041201.

